

## A Numerical Study of the Along-Line Variability of a Frontal Squall Line during PRE-STORM

STÉPHANE BÉLAIR

*Recherche en Prévision Numérique, Environment Canada, Dorval, Quebec, Canada*

DA-LIN ZHANG

*Department of Meteorology, University of Maryland, College Park, Maryland*

(Manuscript received 5 February 1996, in final form 4 March 1997)

### ABSTRACT

Despite considerable progress in the understanding of two-dimensional structures of squall lines, little attention has been paid to the along-line variability of these convective systems. In this study, the roles of meso- and larger-scale circulations in the generation of along-line variability of squall lines are investigated, using an 18-h prediction of a frontal squall line that occurred on 26–27 June 1985 during PRE-STORM (Preliminary Regional Experiment for Stormscale Operational Research Meteorology). It is shown that the Canadian regional finite-element (RFE) model reproduces reasonably well a number of surface and vertical circulation structures of the squall system, as verified against available network observations. These include the initiation, propagation, and dissipation of the squall system, surface pressure perturbations, and cold outflow boundaries; a midlevel mesolow and an upper-level mesohigh; a front-to-rear (FTR) ascending flow overlying an intense rear-to-front (RTF) flow; and a leading convective line followed by stratiform precipitation regions.

It is found that across-line circulations at the northern segment of the squall line differ significantly from those at its southern segment, including the different types of precipitation, the absence of the RTF flow and midlevel mesolow, and the early dissipation of organized convection in the northern part. The along-line variability of the squall's circulations results primarily from the interaction of convectively generated perturbations with a midlevel baroclinic trough. The large-scale trough provides an extensive RTF flow component in the southern portion of the squall system and an FTR flow component in the north, whereas the midlevel mesolow tends to enhance the RTF flow to the south and the FTR flow to the north of the mesolow during the mature to decaying stages. The along-line variability of the squall's circulations appears to be partly responsible for the generation of different weather conditions along the line, such as the development of an upper-level stratiform region in the southern segment and a midlevel cloud region in the northern portion of the squall line.

### 1. Introduction

Considerable progress has been made in recent years on the understanding of two-dimensional structures and evolution of midlatitude squall lines. These mesoscale convective systems (MCSs) often exhibit a line of deep convection, followed by a region of stratiform precipitation (e.g., Ogura and Liou 1980; Smull and Houze 1985, 1987; Johnson and Hamilton 1988; Biggerstaff and Houze 1991a). Their internal flow structures are characterized by a front-to-rear (FTR) ascending current of higher equivalent potential temperature  $\theta_e$  air overlying an elevated or descending rear-to-front (RTF) flow of low- $\theta_e$  air (e.g., Moncrieff 1981; Smull and Houze 1985, 1987; Rutledge et al. 1988; Zhang and Gao 1989).

Midlevel mesovortices or intense cyclonic vorticity concentrations (Stirling and Wakimoto 1989; Brandes 1990; Bartels and Maddox 1991; Biggerstaff and Houze 1991b; Zhang 1992), as well as midlevel mesolows (Zhang and Gao 1989; Biggerstaff and Houze 1991a; Lin and Johnson 1994) and upper-level mesohighs (Zhang and Gao 1989; Gallus and Johnson 1992), have been found to develop in the trailing stratiform regions. Most of these features, organized on the meso- $\beta$ -scale (i.e., order of 20–200 km; Orlanski 1975), have been summarized in the conceptual model of squall lines by Houze et al. (1989).

In contrast, much less attention has been paid to the along-line variability of squall's internal structures, due partly to the limited area of high-resolution observations and partly to the limited capability of numerical weather prediction (NWP) models to resolve multiscale circulations. Recently, the variability of rear inflow jets has been the subject of a few studies. For instance, previous studies showed that the variation of rear inflow intensity

---

*Corresponding author address:* Dr. Da-Lin Zhang, Department of Meteorology, University of Maryland, College Park, MD 20742-2425.  
E-mail: dalin@atmos.umd.edu.

could be related to convectively induced midlevel mesolows (Smull and Houze 1987) or mesovortices (Zhang 1992); namely, it is stronger (weaker or absent) to the south (north) of a midlevel mesovortex. Thus, Zhang (1992) postulated to visualize the midlevel mesoscale rear inflow jet as part of the vortex circulation. Davis and Weisman (1994) and Skamarock et al. (1994) simulated squall lines that exhibit asymmetric circulations in the vicinity of mesovortices when the effect of earth rotation is included. Such three-dimensional flow structures even arise at the convective scale, as demonstrated by Weisman (1993), in which rear inflow jets are enhanced in the middle of a convective bow-echo line due to the development of meso- $\gamma$ -scale (i.e., order of 2–20 km; Orlanski 1975) vortices at the ends of the line (i.e., bookend vortices). Klimowski (1994) noted from dual-Doppler analyses that the rear inflow jet is stronger in regions of high-reflectivity cores, confirming the importance of convective-scale forcing.

Similarly, little attention has been paid to the role of large-scale flows, which normally influence the development and organization of deep convection along squall lines. In particular, squall lines often occur in the vicinity of midlevel short-wave troughs or upper-level jet streams (e.g., Ogura and Liou 1980; Srivastava et al. 1986; Leary and Rappaport 1987; Johnson and Hamilton 1988; Carbone et al. 1990). Thus, we should expect that the internal circulation structure of squall lines may vary, depending on their location with respect to the large-scale disturbances. For instance, the circulation of a squall line that develops at the base of a baroclinic trough, where the RTF ambient flow is stronger, could differ from that of a squall line that occurs to the north of the base or ahead of the trough. In this regard, Zhang and Gao (1989) showed the importance of a large-scale RTF flow component associated with an upper-level jet stream prior to the development of the 10–11 June 1985 PRE-STORM (Preliminary Regional Experiment for STORM-Central; see Cuning 1986) squall line. This has been recently confirmed by Yang and Houze (1995) and Gallus and Johnson (1995), who could only simulate half of the RTF flow intensity associated with the 10–11 June squall system, without inclusion of the large-scale forcing in their model initial conditions. In other cases, however, such a large-scale support may be less obvious, particularly for mesoscale convective systems (MCSs) in which rear inflows are weak and less extensive (see Smull and Houze 1987). Nevertheless, even within a single linear squall system with a length scale of several hundred kilometers, the vertical circulation at one location would differ from that at other locations when it is embedded in a large-scale curved flow.

The purpose of the current study is to address the roles of meso- and larger-scale circulations in the generation of variable (meso- $\beta$ -scale) internal structures (e.g., FTR and RTF flows, mesolows and mesohighs, stratiform regions) within midlatitude squall lines, using an 18-h simulation of a frontal squall system that oc-

curred on 26–27 June 1985 during PRE-STORM. This squall system has been documented by Trier et al. (1991) and Lin and Johnson (1994). They showed that the squall line, having a length scale of 1500–1800 km, developed ahead of a surface cold front with a pronounced baroclinic trough aloft. Their analyses also revealed the development of an upper-level stratiform region at the rear of the squall system, with classic two-dimensional flow structures as described earlier. Moreover, Lin and Johnson (1994) noted two different types of RTF flows: an elevated one that intensified in response to the development of a midlevel mesolow (Smull and Houze 1987) and a surface-based one that was related to the cold frontal circulation. These two observational analyses provide useful information on the understanding and model verification of the 26–27 June squall system for the current study. They are, however, limited to only the southern segment of the squall system that was covered by the PRE-STORM network. It remains uncertain whether similar across-line circulations would develop at the northern segment of the squall line. If not, what are the roles of the meso- and larger-scale circulations in determining the different internal structures of the squall system? Thus, the primary objectives of this study are to 1) examine the mesoscale predictability of variable meso- $\beta$ -scale circulations of the 26–27 June 1985 squall line using a high-resolution research version of the Canadian regional finite-element (RFE) model, 2) investigate the along-line variability of organized deep convection and the squall's internal structures, and 3) clarify the multiscale interactions involved in the development of rear inflow and FTR flows in the current squall line.

The presentation of the results is organized as follows. The next section discusses briefly the main features of the RFE model and the initial conditions. Section 3 provides verification of the 18-h model prediction against available observations and examines the two-dimensional vertical structure of the squall line. Section 4 describes the model results that are related to the along-line variability of the organized convection, as well as its associated prestorm environment. In sections 5 and 6, we investigate the along-line variability of the meso- $\beta$ -scale structures and weather conditions of the simulated squall system due to meso- and larger-scale circulations, respectively. A summary and concluding remarks are given in the final section.

## 2. Model description and initial conditions

An improved version of the RFE model is used for this study, with a high-resolution uniform grid interval of 25 km over the central domain covering most of the United States and southern Canada; outside this central domain, the grid size increases by a constant factor ( $\sim 14\%$ ) in every direction until the equator is reached (see Fig. 1). Table 1 summarizes the basic model features; they are the same as those used in Bélair et al.

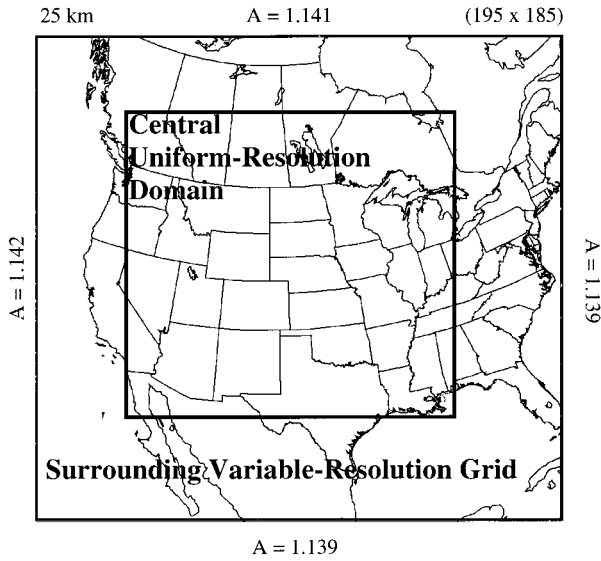


FIG. 1. Portion of the  $195 \times 185$  hemispheric variable grid mesh projected on a polar stereographic plane. The heavy rectangle indicates the central uniform high-resolution domain of 25 km with the grid size increasing by constant amplification factors  $A$  in every direction.

TABLE 1. Summary of the mesoscale RFE model.

Numerics

- 3D, hydrostatic, primitive equations
- Semi-implicit time discretization
- Semi-Lagrangian scheme for three-dimensional advection (time step: 300 s)
- Linear finite elements in  $(x, y, \sigma)$
- Variable horizontal resolution grid overlaid on a polar stereographic projection (25 km in fine mesh grid)
- 19  $\sigma$  levels with high resolution in the lowest 150 hPa
- Second-order horizontal diffusion for temperature, vorticity, and divergence
- $0.5^\circ$  orography field

Physics

- Planetary boundary layer (PBL) based on turbulent kinetic energy
- Diagnostic PBL height
- Implicit vertical diffusion
- Surface energy budget based on force–restore method
- Diurnal cycle with solar and infrared fluxes at the ground modulated by clouds
- Infrared and solar radiation fluxes calculated at all levels
- Diagnostic cloud cover
- Fritsch–Chappell scheme for parameterized moist convection
- Explicit moisture scheme containing prognostic equations for cloud water (ice) and rainwater (snow)

(1994, 1995). Briefly, the RFE model incorporates a modified version of the Fritsch and Chappell (1980; hereafter referred to as FC) convective parameterization scheme (Zhang and Fritsch 1986), which is coupled with an explicit moisture scheme predicting cloud water (ice) and rainwater (snow) (Hsie et al. 1984; Dudhia 1989; Zhang 1989). This version of the model is similar to that used operationally at the Canadian Meteorological Center (CMC), except for the above physics package and the high-resolution grid length. The model is initialized at 1200 UTC 26 June 1985 with conventional meteorological observations using the same procedures as those described in Bélair et al. (1994). No supplementary data were treated for the model initialization, since the PRE-STORM network did not collect detailed observations until 1800 UTC 26 June when the squall line under study was initiated.

At the model's initial time, a large-scale surface cold front extends from western Texas to western Ontario, with a low pressure zone located over western central Kansas (see Fig. 2). The surface circulation shows an anticyclonic northerly cold current associated with the high pressure center over Wyoming and a warm moist southerly flow ahead of the cold front; the two air currents converge along the front. As will be shown in section 4, the prefrontal environment is conditionally unstable, with convective available potential energy (CAPE) of approximately  $2500 \text{ J kg}^{-1}$  (see Fig. 11). This prefrontal environment, in conjunction with thermally direct circulations associated with frontogenesis (Trier et al. 1991), provides favorable conditions for the development of deep convection 6 h later. At 500 hPa, a large-amplitude baroclinic trough corresponding to the

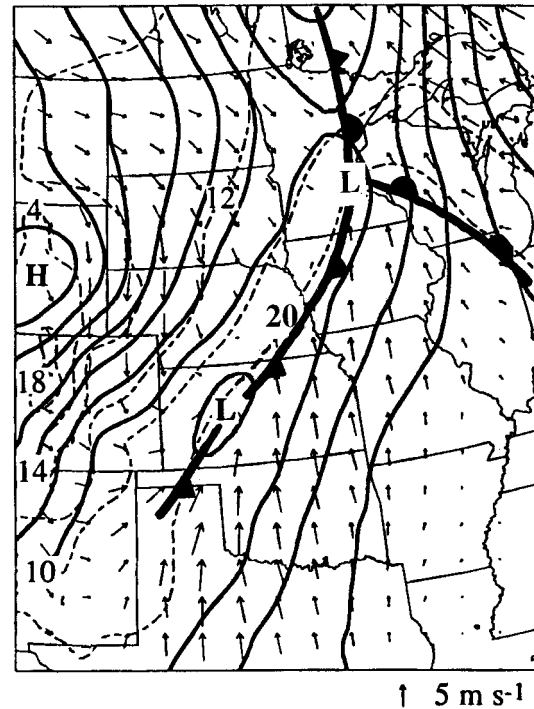


FIG. 2. Model initial conditions: Sea level pressure (solid, every 2 hPa) superposed with the surface wind vectors and temperature (dashed, every  $4^\circ\text{C}$ ) at 1200 UTC 26 June 1985. The surface frontal positions are determined from the detailed surface analysis of Trier et al. (1991).

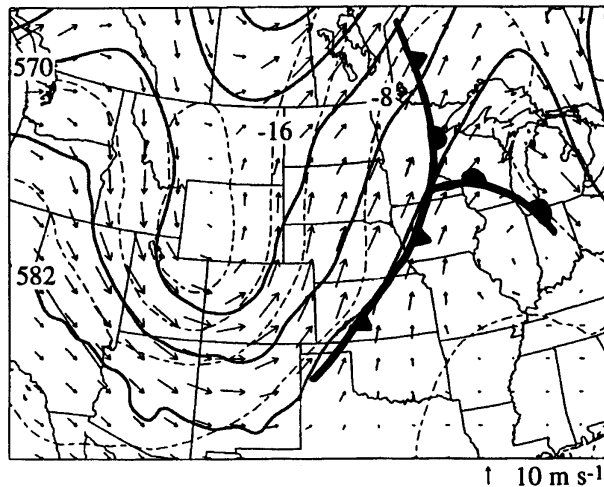


FIG. 3. As in Fig. 2 but for 500-hPa geopotential height (solid, every 6 dam) and temperature (dashed, every 4°C), superposed with horizontal wind vectors.

surface front is present (Fig. 3), with the base of the trough located just upstream of the PRE-STORM network (i.e., over Kansas and Oklahoma). Note that the midlevel flow associated with the trough is nearly equivalent barotropic, whereas the prefrontal flow is nearly barotropic (i.e., having little gradient). For additional details on the environmental conditions, the reader is referred to Trier et al. (1991).

### 3. Model verification

Before examining the variable internal structures of the 26–27 June squall line, it is important to ensure that the RFE model reproduces reasonably well the basic structures and evolution of the system as verified against all available observations. In this section, radar summaries, rawinsonde observations, Doppler data, satellite imagery, and surface analyses are used to help validate the model prediction and describe the general evolution of the squall system. In the following subsections, we verify the prediction of surface features, including precipitation, area of organized convection, sea level pressure, and temperature fields, and then investigate the predicted tropospheric structures of the squall system.

#### a. Surface features

The squall line was initiated ahead of the surface cold front over Nebraska and Kansas at about 1800 UTC 26 June (Trier et al. 1991), that is, 6 h into the integration, hereafter 26/18–06. Then, as the daytime boundary layer developed, the convective activity expanded rapidly north- and southward along the front, leading to the generation of a long and intense line of deep convection that extended from Texas to Lake Superior by 27/00–12 (see Figs. 4a and 5a). Precipitation also occurred behind the convective line, that is, over South Dakota,

in association with the lower-level cloudiness visible in the satellite imagery (cf. Figs. 4a and 5a). The convective activity in the southern portion of the squall line, which was located over the PRE-STORM network, weakened after 27/00–12, but it still remained well organized even at 27/06–18 [see Figs. 4b and 5b herein and Figs. 3e–h in Lin and Johnson (1994)]. In contrast, the northern portion of the convective system was almost completely dissipated by 27/06–18. Only a notable area of precipitation was found to the rear of this northern segment, that is, over North and South Dakota (Figs. 4b and 5b).

The model predicts well the initiation of the squall line at nearly the right time and location (not shown), as well as the distribution and orientation of convective activity along the squall line during the mature (i.e., 27/00–12) to dissipating (i.e., 27/06–18) stages (cf. Figs. 4 and 5). Although it lags slightly behind the observed, the long line of parameterized convection at the mature stage agrees well with 1) the radar summary chart showing echo tops up to 40 000 ft (12 km, Figs. 4a,b), 2) the satellite imagery (Fig. 5a), and 3) the radar reflectivity over the PRE-STORM network (see Fig. 3d in Lin and Johnson 1994). Most of the predicted precipitation is convective at this stage (not shown). The subsequent disintegration and maintenance of the squall system at its respective northern and southern segments are also well reproduced by the model (cf. Figs. 4b and 4d). Note that even after the northern portion of the squall system dissipated, deep but localized convective systems were still present along the front (cf. Figs. 4c, d). The model also reproduces two trailing precipitation regions at the mature to dissipating stages: one over Minnesota and the other over Oklahoma [cf. Figs. 4b, 4d, and 5b herein, and Fig. 4h in Lin and Johnson (1994)].

As the squall system intensified, significant changes also took place at the surface, except for the high pressure zone over Wyoming, which was nearly quasi-stationary (see Figs. 6a,b). For example, a pressure ridge, extending from the high pressure zone into central Oklahoma, was enhanced by diabatic cooling behind the convective line. One effect of this ridge was to split the frontal trough into two parts: one was the original mesolow being pushed northeastward and the other was a presquall mesotrough at the southern end of the squall system. Another effect of the intense evaporatively driven cold outflow, which was more evident during the daytime to the south of the surface mesolow, was to accelerate the movement of the (southern) squall line; it propagated at a speed of  $8.6 \text{ m s}^{-1}$  (Lin and Johnson 1994), which was much faster than its northern counterpart (i.e.,  $4 \text{ m s}^{-1}$  between 27/00–12 and 27/03–15). By 27/06–18, the southern portion of the squall line had traversed the PRE-STORM network.

A comparison between Figs. 6a,b and 6c,d indicates that the RFE model reproduces reasonably well the main surface features during the mature and dissipating

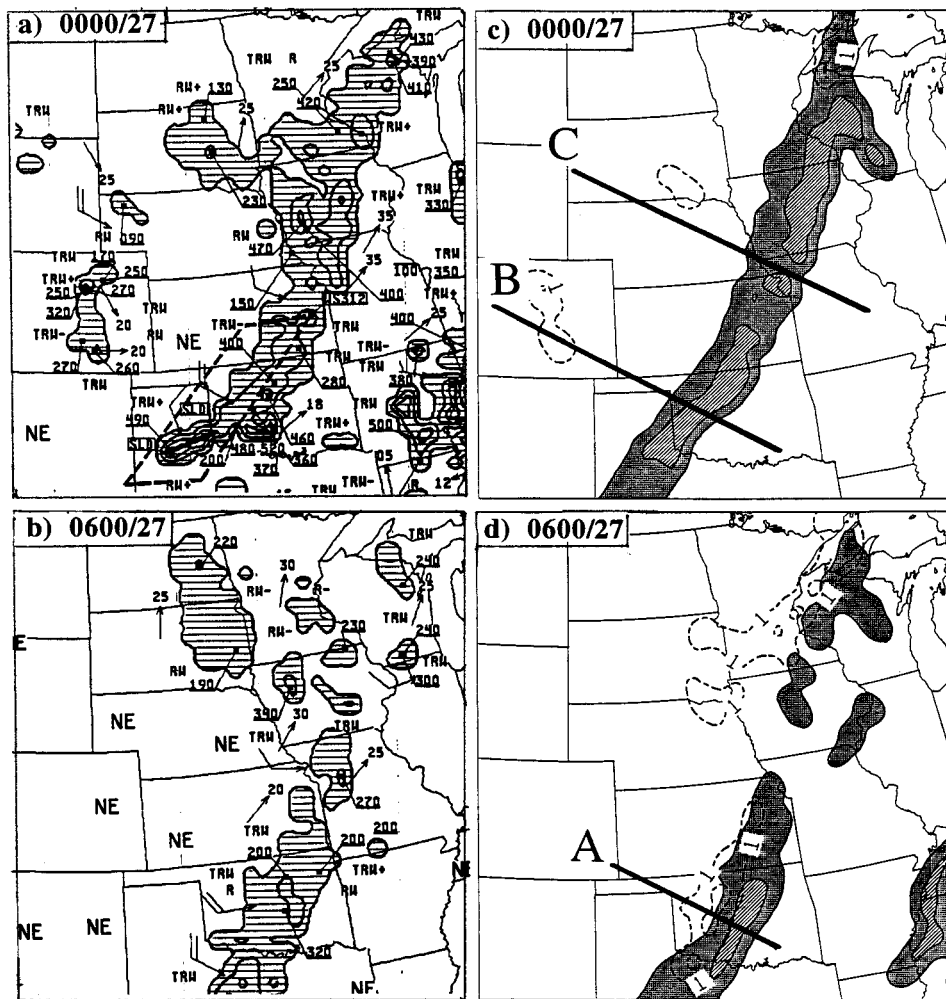


FIG. 4. Left panels show radar summary charts at (a) 0000 UTC and (b) 0600 UTC 27 June 1985. Right panels show the predicted grid-scale (dashed) and parameterized (shaded) rainfall rates with contours of 1 and 5 mm h<sup>-1</sup> from (c) 12-h (27/00–12) and (d) 18-h (27/06–18) integrations.

stages, such as the low and high pressure centers over Iowa and Wyoming, the presquall mesotrough, and the cold outflow boundary. The model also captures reasonably well the orientation and propagation of the squall front (9 and 4 m s<sup>-1</sup> for the southern and northern segments, respectively), which are strongly influenced by parameterized moist downdrafts in the FC scheme. The predicted squall front, however, exhibits a little weaker intensity than the observed at the formative stage, thereby causing the slightly slower movement of the gust front, especially for the southern segment of the squall system. The weaker intensity appears to be caused partly by the (3°–4°C) underprediction of surface temperature in the cloud-free region ahead of the cold front and partly by the less cold downdraft air in the FC parameterization.

It should be mentioned that there are several other deficiencies with the 18-h model prediction. For example, the model appears to have delayed the precipi-

tation production over Arkansas by 6 h; similar results were obtained for the precipitation over North and South Dakota (see Fig. 4). Due to its relatively coarse grid size, the model is unable to resolve some small-scale features, such as the multiple convective lines and their associated pressure perturbations ahead of the surface front as described in Trier et al. (1991). Nevertheless, the above results show that the RFE model captures reasonably well the main features of the squall line, and it can therefore be used in the following sections to investigate some meso- $\beta$ -scale structures of the system and the mechanisms responsible for the along-line variability of the squall's internal circulations.

#### b. Tropospheric structures

It is apparent from Fig. 7 that the model could reproduce well some typical meso- $\beta$ -scale structures of the squall line during the mature and dissipating stages.

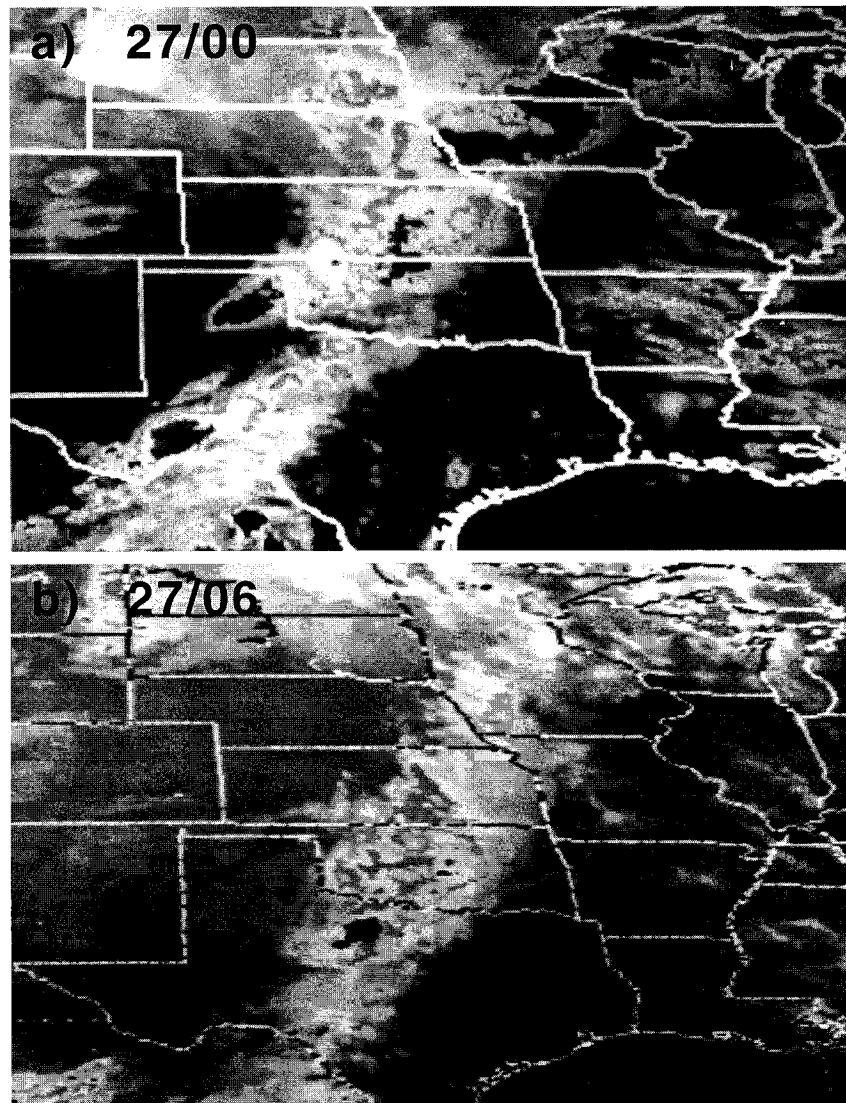


FIG. 5. Satellite infrared imagery at (a) 0000 UTC and (b) 0600 UTC 27 June 1985.

Specifically, a strong FTR ascending flow occurs within a deep, near-saturated layer from the leading convective line to the trailing stratiform region; its trailing segment at upper levels extends rearward a few hundred kilometers. This near-saturated region is characterized by negative moist potential vorticity (MPV) (not shown), implying the presence of moist symmetric instability. This instability develops as a result of transporting potentially unstable air from the presquall boundary layer into the FTR sloping ascent region, after being stabilized by upright convection at the leading line, a process as described by Zhang and Cho (1992). Beneath the stratiform cloudiness, a system-relative RTF current with a maximum speed of  $16 \text{ m s}^{-1}$  transports extremely dry midlevel air (with minimum relative humidity of less than 10%) into the system, thereby causing intense sublimative and evapo-

rative cooling and descent near the leading edge of the current. This cold downdraft air penetrates into the boundary layer at the leading edge of the squall line and forms the surface squall front at which strong convergence occurs between the FTR and RTF currents. In some cases (e.g., the 10–11 June squall system), surface mesolows may form at the back edge of the stratiform region when adiabatic warming associated with the RTF descending flow exceeds diabatic cooling (see Johnson and Hamilton 1988; Zhang and Gao 1989). In the current case, however, both the prediction and the observations show a mesoridge or a weak mesohigh behind the system (see Figs. 6b,d), indicating that diabatic cooling within the RTF descending current dominates. The development of wake lows appears to depend on the intensity of RTF descending flow, the low-level thermal lapse rates and moisture content, and

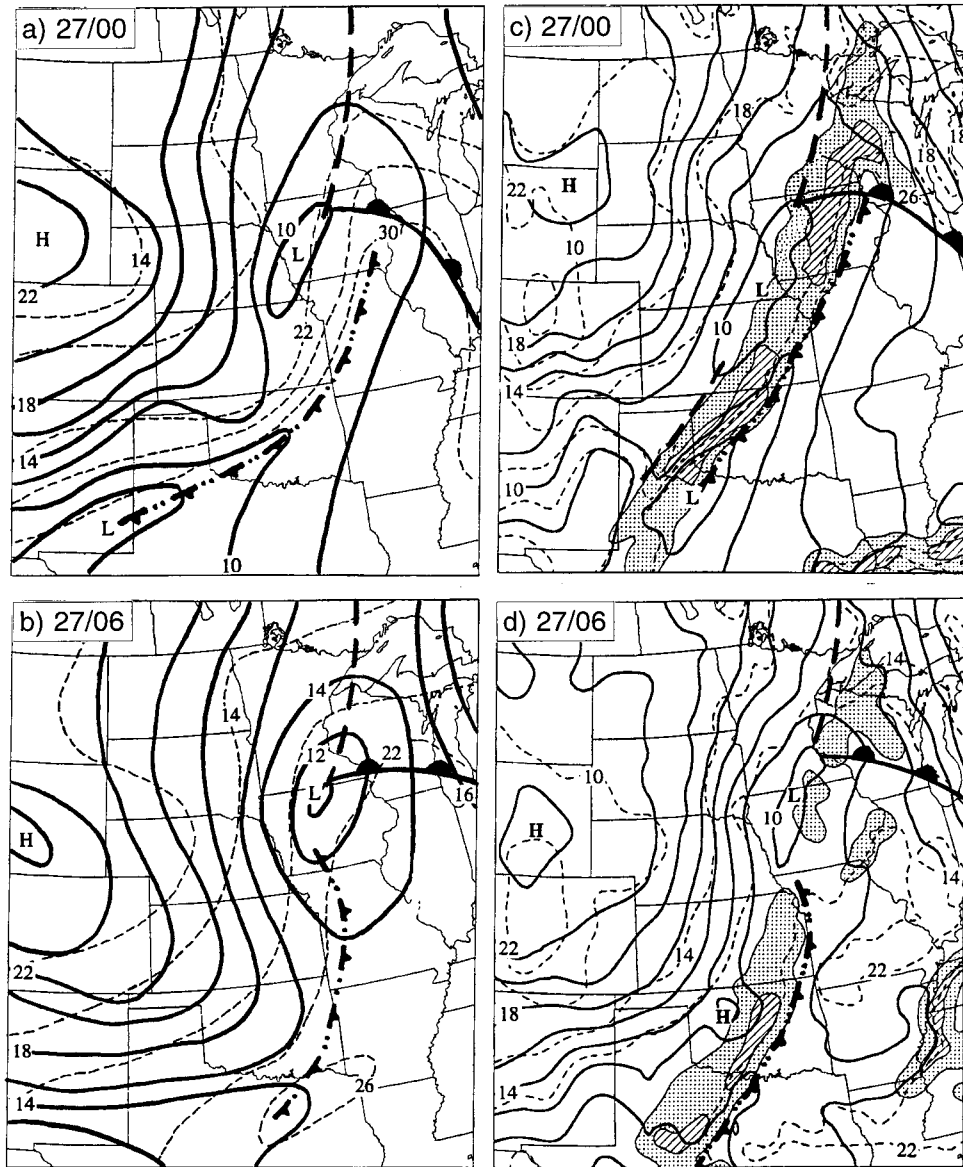


FIG. 6. Left panels show sea level pressure (solid, every 2 hPa) and surface temperature (dashed, every 4°C) at (a) 0000 UTC and (b) 0600 UTC 27 June 1985. Right panels show the corresponding fields from (c) 12-h (27/00–12) and (d) 18-h (27/06–18) integrations. Shadings show the predicted parameterized convective rainfall rates with contours of 1 and 5 mm h<sup>-1</sup>. Cold-frontal symbols with double dots indicate outflow boundaries.

the propagation of a squall system, as well as the intensity of large-scale baroclinicity.

The above circulations compare favorably to the 2D representations of the squall system analyzed by Trier et al. (1991) and Lin and Johnson (1994). For instance, the Doppler radar analysis by Trier et al. (1991) shows the existence of a well-developed couplet of FTR and RTF currents as early as 27/00–12 (see their Fig. 21). Similar flow structures were observed by the PRE-STORM upper-air network (see Figs. 4 and 9 in Lin and Johnson 1994). However, Lin and Johnson's analysis shows that 1) the midlevel RTF flow was very weak

during the mature stage (i.e., 27/00–12) and strong at later stages when a midlevel mesolow formed, and 2) the rear inflow jet never extended forward into the leading convective line, as it did in the RFE prediction (see Fig. 7). These discrepancies, particularly for the descending portion of the RTF flow, appear to be attributable partly to the limited resolution of rawinsonde observations and partly to the along-line averaging length scale (about 300 km) they used.

Figure 8 compares the predicted geopotential heights and horizontal winds at 700 hPa to the observed during the system's dissipating stages. The RFE model captures

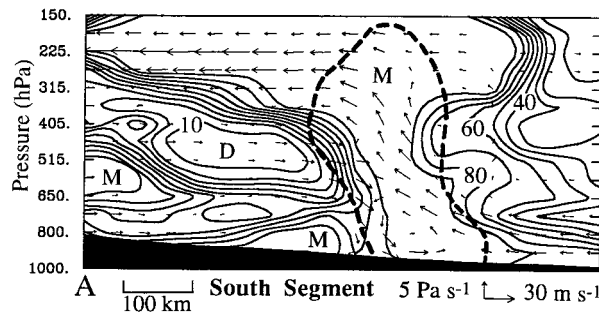


FIG. 7. Vertical cross section of relative humidity (solid, every 10%), superposed with line-normal relative flow vectors, taken from 18-h integration (27/06–18) along line A (through the south segment) given in Fig. 4d. Thick dashed line denotes the precipitable water contour of 0.1 g kg<sup>-1</sup>. Letters “D” and “M” indicate dry and moist centers, respectively.

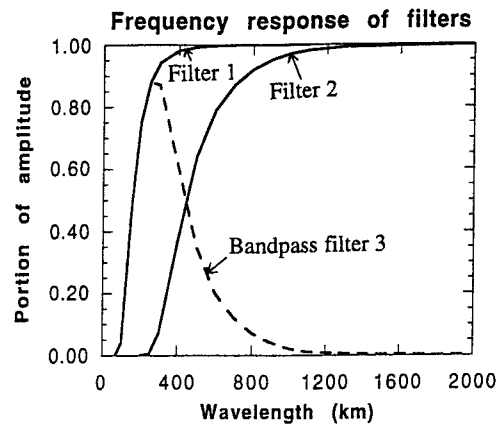


FIG. 9. Portion of returned amplitude vs wavelength (km) by the low-pass filters 1 and 2 and the bandpass filter 3.

well two scales of circulations, that is, a large-scale trough, in which the squall system is embedded, and a mesolow in the trailing stratiform region of the system. Their orientations and relative locations are reasonably reproduced. Lin and Johnson (1994) also noted the development of such a midlevel low pressure zone during the dissipating stages. As will be discussed in sections 5 and 6, these two scales of circulations have significant implications with respect to the along-line variability of internal flow structures and weather conditions along the front.

For the sake of subsequent discussions, it is necessary to separate the mesoscale from the large-scale signals and determine the relationship between the squall development and the mesoscale pressure disturbances. These can be achieved by applying a simple scale-separation technique similar to that utilized by Maddox

(1980a) to the height and temperature fields. First, the two fields are spatially filtered on two horizontal grid meshes with different resolutions (see filters 1 and 2 in Fig. 9). The low-resolution grid mesh (filter 2) only represents disturbances with wavelengths longer than 500 km (i.e., larger scale), whereas all the wavelengths greater than 150 km (i.e., meso- and larger scale) are included on the high-resolution grid mesh (filter 1). Then, a bandpass filter is obtained by subtracting the results of filter 2 from filter 1, thus yielding the characteristics of convectively generated perturbations on the scale of 150–500 km. It is evident from Figs. 10a,b that this scheme isolates well the vertical structure of mesoscale perturbations in the vicinity of the squall system from the larger-scale circulations. A midlevel mesolow and an upper-level mesohigh associated with the squall system are centered at locations where conver-

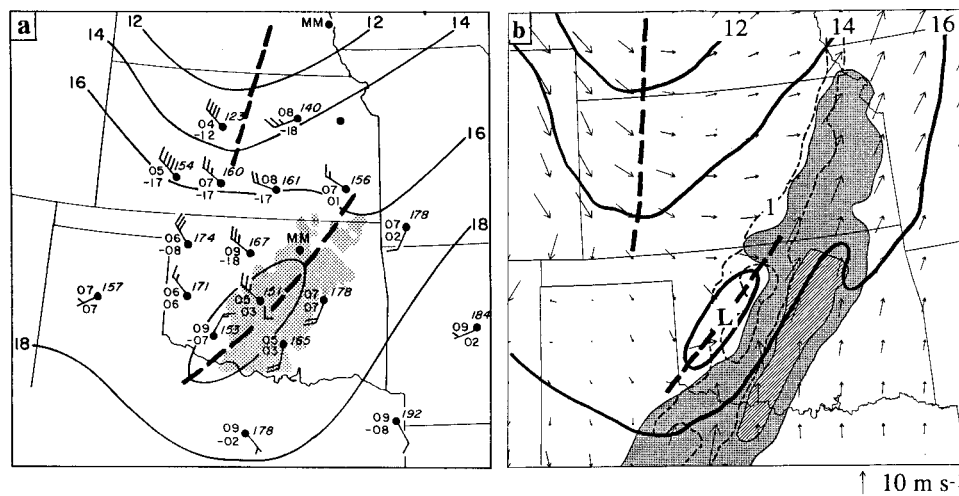


FIG. 8. Horizontal maps of 700-hPa geopotential height (solid, every 2 dam) from (a) the analysis (courtesy of S. Trier), superposed with wind barbs (a full barb is 5 m s<sup>-1</sup>) and radar echo at 0600 UTC 27 June; and (b) 18-h integration (27/06–18), superposed with wind vectors and grid-scale (dashed) and parameterized convective (shadings) rainfall rates with contours of 1 and 5 mm h<sup>-1</sup>. Note that the height values are in excess of 300 dam (i.e., 12 = 312 dam).

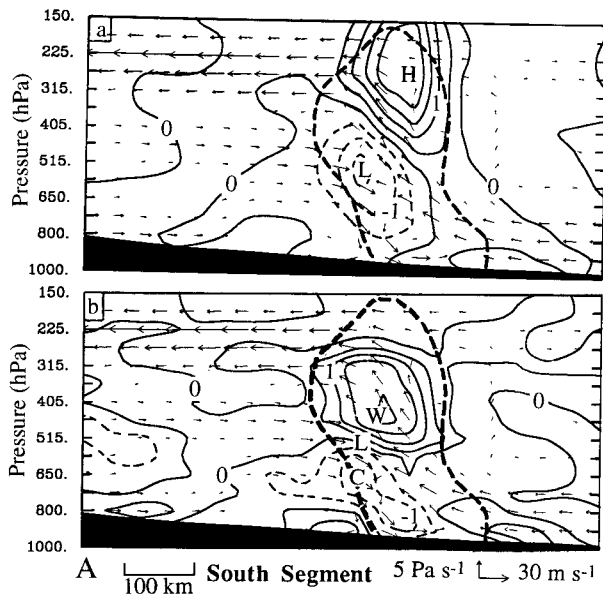


FIG. 10. As in Fig. 7 but for (a) mesoscale height perturbations (every 5 dam); and (b) temperature perturbations (every  $0.5^{\circ}\text{C}$ ). Solid (dashed) lines are positive (negative) values. Letters “L” and “H,” “W” and “C” denote the centers of the mesolow and mesohigh, warming, and cooling, respectively.

gence and divergence are maximized, respectively. Apparently, the midlevel mesolow is hydrostatically produced by net warming in the FTR ascending flow and evaporative–sublimative cooling in the RTF descending flow, with its center situated at the interface between the warming above and cooling below, as has also been found by Zhang and Gao (1989) and Braun and Houze (1994). In contrast, the upper-level mesohigh is produced by the net adiabatic and parameterized detrainment cooling above the intense updrafts and the net warming below. Such an upper-level mesohigh has been frequently observed (e.g., Fritsch and Maddox 1981a; Fritsch and Brown 1982; Maddox et al. 1981; Gallus and Johnson 1992) and simulated by other NWP models (e.g., Fritsch and Maddox 1981b; Gao et al. 1990). This feature can also be seen from the analysis of Lin and Johnson (1994).

#### 4. Along-line variability of deep convection

We have seen from Figs. 4 through 6 that the southern and northern segments of the squall line differ significantly in the longevity and organization of deep convection. The convective activity remained well organized in the southern segment at 27/06–18, but it dissipated shortly after 27/00–12 for the northern part. Thus, it is desirable to study first the along-line variability of organized deep convection before discussing the variable meso- $\beta$ -scale circulations of the squall system. Previous observational studies have also noted the along-line variability of convective initiation, internal structures, intensity, and movements of squall lines

(e.g., Newton and Fankhauser 1964; Hane et al. 1987). With the present 25-km grid size, it is impossible to investigate the along-line variability of convective cells as well as their interactions with prestorm environments. However, it is appropriate to examine the collective initiation of deep convection and its mesoscale organization using the model prediction, since the RFE model with the FC scheme reproduces very well the integral effects of deep convection along the squall line. In the FC convective scheme, parameterized convection is triggered when 1) grid-scale upward motion is strong enough to lift a parcel from the boundary layer to the level of free convection, and 2) the atmospheric column in which the parcel is lifted is conditionally unstable. With the FC scheme, NWP models have been shown to be capable of reproducing the development of many meso- $\beta$ -scale structures of MCSs (e.g., Zhang and Fritsch 1986, 1988; Zhang and Gao 1989; Zheng et al. 1995).

To help understand the along-line variability of organized deep convection, Figs. 11a, b show two composite presquall soundings at the respective southern and northern segments prior to the squall system’s disintegration (i.e., 27/00–12). Here, the two composite soundings are generally similar in character, both exhibiting a well-developed daytime boundary layer, small convective inhibition (CIN), large CAPE, weak to negative vertical shears normal to the line in the lowest 200 hPa, and a high level of equilibrium temperature (i.e., 160 hPa). Although the well-mixed boundary layer in the north is slightly shallower, the general presquall thermodynamic conditions do not appear to cause the early dissipation of the northern convective activity. In fact, the CAPE in the north segment ( $3300 \text{ J kg}^{-1}$ ) is greater than that in the south ( $2500 \text{ J kg}^{-1}$ ), and the CIN is relatively smaller (cf. Figs. 11a,b), indicating that the triggering and organization of deep convection should be less constrained to the north if other conditions are identical. Furthermore, the modeled gridpoint soundings are still conditionally unstable even over the dissipated convective region to the north at later times (not shown). It is quite possible that the interaction of convective-scale downdrafts with prefrontal wind shear may be less favorable for organized development (Rotunno et al. 1988). This does not seem to be the case on the current grid scale (25 km), since the model with the parameterized convection, in which such an interactive process is not included, reproduces well the dissipation of deep convection in the north.

An examination of the grid-scale forcing reveals that the longevity and organization of parameterized deep convection are determined more by the convergence in the boundary layer where deep convection is rooted. Specifically, the convergence is more intense along the southern portion of the squall system where the divergent cold current, enhanced by convectively generated cold downdrafts, meets the southerly flow along the cold front (see Fig. 12), making the initiation of parameter-

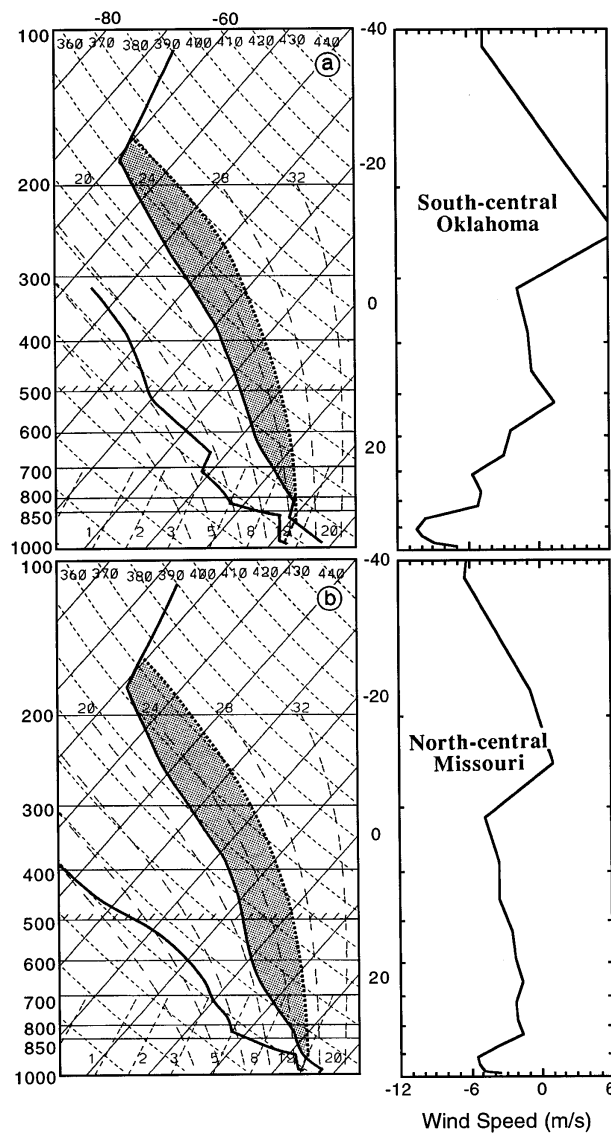


FIG. 11. Skew  $T$ -log $p$  diagrams showing prefrontal tropospheric soundings from 12-h integration (27/00–12). The soundings were obtained by averaging five grid points located between 50 and 150 km ahead of the leading precipitation line along (a) line B (i.e., over south-central Oklahoma) and (b) line C (i.e., over north-central Missouri) given in Fig. 4c. Shadings show positive CAPE. Composite vertical profile of the line-normal flow is given at the right of the diagrams.

ized convection relatively easier and its organization more sustainable over the region than in the northern segment. The most intense convergence takes place over western Oklahoma ( $-20 \times 10^{-5} \text{ s}^{-1}$ , as compared to  $-8 \times 10^{-5} \text{ s}^{-1}$  in the north) where the two currents with opposite directions intersect across the cold front, leading to the strong lifting of high- $\theta_e$  air from the south (see Fig. 7), whereas their line-normal components decrease away from the region, more markedly northward along the cold front.

One may wonder how such variable low-level forcing

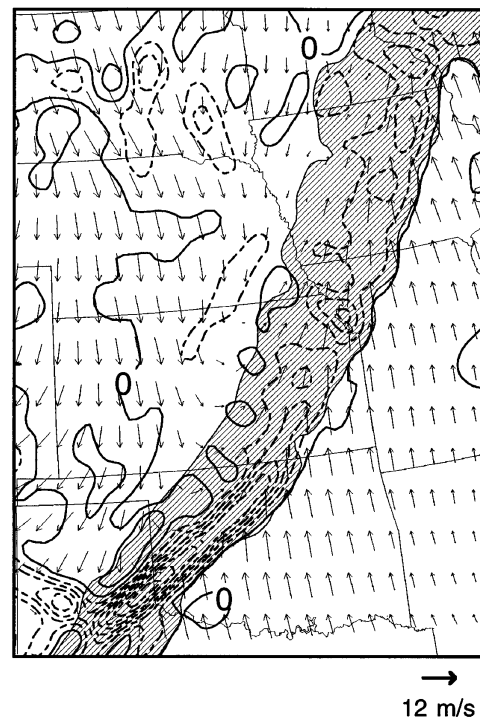


FIG. 12. Horizontal map of divergence (every  $4 \times 10^{-5} \text{ s}^{-1}$ ) at  $\sigma = 0.95$ , superposed with wind vectors, from 12-h integration (27/00–12). Solid (dashed) lines are for positive (negative) values. Shadings show the convective rainfall rates greater than  $1 \text{ mm h}^{-1}$ .

structures could develop from the larger-scale flows that are relatively uniform in the vicinity of the squall line (cf. Figs. 3 and 6). This could be understood, in part, using the absolute momentum conservation principle. Namely, as the midlevel RTF (FTR) flow descends (ascends), it will be deflected to the right by the local Coriolis force. Hence, the surface cold current (over eastern Oklahoma) could be related partly to the mid-level (RTF) flow behind the trough axis (see Figs. 3 and 15), as the colder air descends anticyclonically toward the surface. Note, though, that the large-scale northerly flow in the current case may be influenced partly by the channeling effect of the Rocky Mountains. It is evident that there will be little variability if it occurs only in two dimensions. It follows that the along-line variability of organized convection is mainly determined by the along-line variability in the low-level across-frontal flows, influenced by the midlevel descending flow and the large-scale northerly current parallel to the mountains, given the relatively uniform presquall environment.

### 5. Along-line variability due to large-scale circulation

We have shown that the southern segment of the squall system, that is, over the PRE-STORM network, contains many meso- $\beta$ -scale structures that are similar

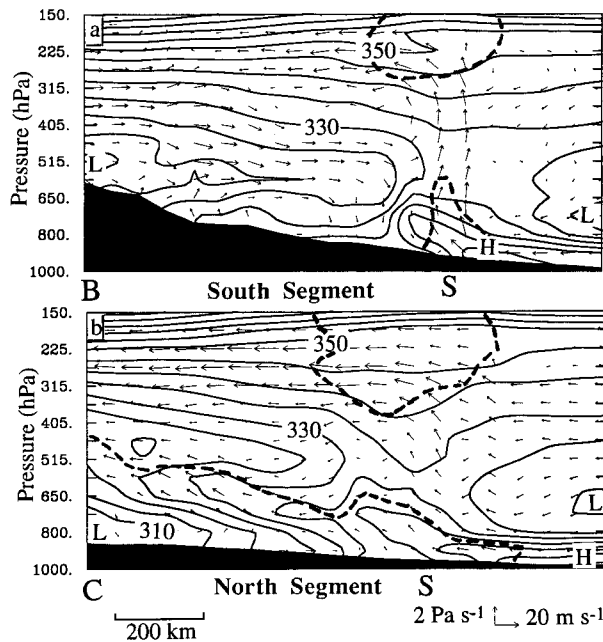


FIG. 13. Vertical cross sections of equivalent potential temperature ( $\theta_e$ , every 5 K) with line-normal relative flow vectors, which were taken from 12-h integration (27/00–12) along (a) line B (through the south segment), and (b) line C (through the north segment) given in Fig. 4c. Letters “L” and “H” show the respective minima and maxima of  $\theta_e$ , and letter “S” shows the position of the squall line. Thick dashed lines indicate regions with relative humidity exceeding 90%.

to those in the conceptual model of midlatitude squall lines (Houze et al. 1989). In this section, we investigate whether these classic structures would appear at other portions of the squall line and then clarify the role of large-scale circulation in determining the along-line variability of the squall’s internal flow structures. The effect of convectively generated disturbances will be discussed in the next section.

To help examine the relationship between the along-line variability and larger-scale circulations, Figs. 13a,b compare the two-dimensional flow structures at the southern segment of the squall system to those at the northern segment during the mature stage. One can see that the prestorm environment is potentially unstable everywhere ahead of the cold front, with high- $\theta_e$  air in the lowest 100 hPa (also see Fig. 11). However, the two-dimensional circulations in the northern segment differ significantly from those in the southern one. Specifically, the southern squall system exhibits an RTF descending current that transports midlevel lower- $\theta_e$  air downward into the boundary layer, whereas in the north there is little evidence of the RTF flow. Instead, there are two FTR (southerly) ascending flows that transport boundary layer high- $\theta_e$  air upward: one along the frontal zone into the midtroposphere, causing potential instability in a shallow layer, and the other through organized deep convection into the upper levels (Fig. 13b). These flow structures conform more or less to the development

of more extensive, midlevel clouds in the north (see Figs. 5a,b). In contrast, the stratiform clouds that developed in the south only appear in the upper troposphere, like those described in the Houze et al. (1989) conceptual model. Furthermore, the grid-scale upward motion is more intense at the southern segment of the squall line due to the presence of strong low- to midlevel convergence associated with the RTF–FTR flows; this in turn helps trigger collectively deep convection at the leading edge of the squall system, as discussed in the preceding section. Note that the above-mentioned differences between the southern and northern segments remain similar throughout the squall’s life cycle.

In the next two subsections, we discuss separately the mechanisms that are responsible for the generation of the different two-dimensional circulation structures occurring at the southern and northern segments of the squall system.

#### a. The RTF descending flow in the southern segment

Rear inflow jets have been the focus of considerable research in recent years. Several hypotheses have been put forward to explain the development of rear inflow. For instance, Smull and Houze (1987) hypothesized that rear inflow could be generated by the forward acceleration associated with a convectively induced midlevel mesolow (on the meso- $\beta$ -scale) in the stratiform region and then by a hydrostatic pressure fall underneath warm convective updrafts (on the meso- $\gamma$ -scale) in the leading convective region. Zhang (1992) extended the mesolow hypothesis to a midlevel mesovortex proposition by including the tilting of horizontal vorticity in the presence of descending motion and vertical shear near the back edge of a stratiform region. Lafore and Moncrieff (1989) and Weisman (1992) argued that the meso- $\gamma$ -scale rear inflow may result from an RTF acceleration associated with buoyancy gradients at the rear of convective updrafts. Based on a two-dimensional simulation, Schmidt and Cotton (1990) attributed the development of a rear inflow jet to the downward deflection and channeling of an ambient RTF flow by convectively generated divergent outflow aloft (i.e., the “blocking” effect). Zhang and Gao (1989) showed that an upper-level jet stream could provide a favorable ambient RTF component that is driven downward by sublimative–evaporative cooling and then enhanced by a midlevel mesolow to form a mesovortex with intense mesoscale RTF flow. It is possible that several of the above mechanisms may operate together.

Now let us examine if any of the aforementioned mechanisms could account for the production of the current rear inflow jet. It must be pointed out that the 25-km resolution model cannot resolve the meso- $\gamma$ -scale lows under warm convective updrafts. However, it is unlikely that such small-scale pressure perturbations could play an important role in generating the extensive rear inflow in the current case. By comparison, the mid-

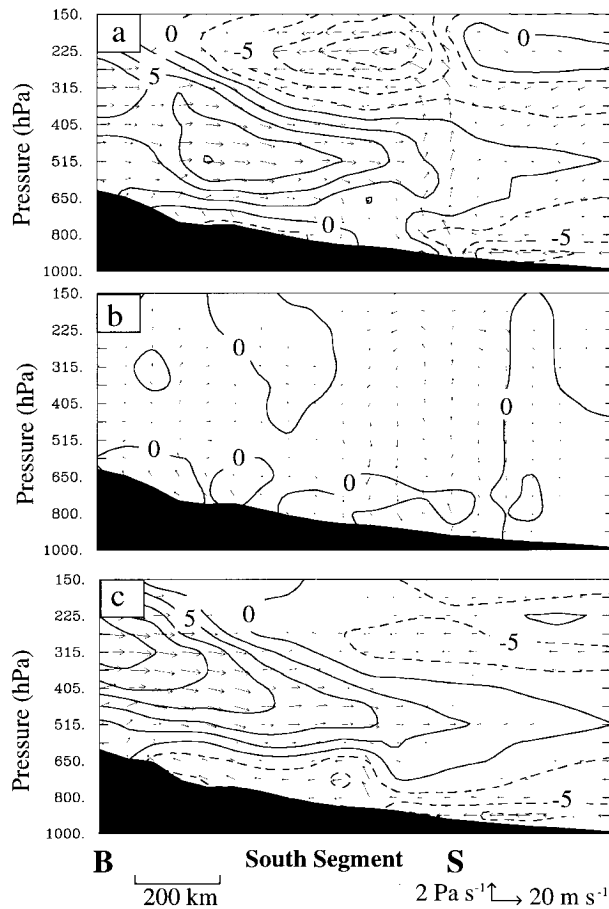


FIG. 14. Vertical cross sections of line-normal relative flow (every  $2.5 \text{ m s}^{-1}$ ), superposed with the flow vectors, taken along line B (the south segment) given in Fig. 4c from 12-h integrations (27/00–12) of (a) experiment CTL; (b) mesoscale circulations as isolated with the scale separation technique from experiment CTL; and (c) experiment DRY.

level meso- $\beta$ -scale low (or mesovortex) can be well resolved by the 2.5-km grid size (see Figs. 8 and 10). But this mechanism does not appear to be significant during the early stages, because the convectively generated mesolow or mesotrough is not evident until the mature to dissipating stages, that is, after 27/03–15, when resolvable-scale precipitation becomes more pronounced.

What about the convective “blocking” or large-scale forcing effects? To help isolate these two processes with different scales, two steps are taken: 1) the scale-separation technique as described previously is applied to the 12-h control simulation (experiment CTL), and 2) a sensitivity experiment is conducted, in which neither convective- nor grid-scale condensation are included (experiment DRY), while keeping all the other physical parameters identical to experiment CTL. It is evident from Figs. 14a,b that convectively generated perturbations at the squall’s incipient stage are negligible compared to the larger-scale contributions. This can be fur-

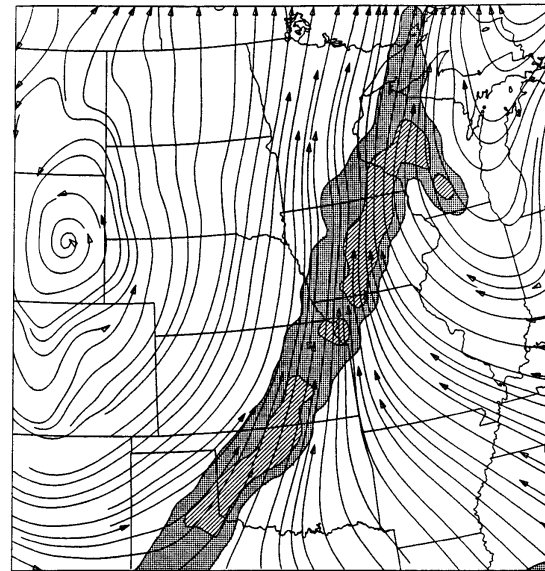


FIG. 15. Horizontal map of 500-hPa system-relative streamlines, superposed with convective rainfall rates (shadings) with contours of 1 and  $5 \text{ mm h}^{-1}$  from 12-h integration (27/00–12).

ther seen by comparing the CTL and DRY runs: an RTF current with the scale and depth similar to those in experiment CTL is also present in experiment DRY (cf. Figs. 14a,c). The basic flow structures between the two runs differ only at upper and lower levels in association with the respective convectively induced divergent outflow and cold descending flow. It follows that the majority of the resolved rear inflow jet at early stages was a manifestation of the large-scale RTF flow rather than the result of mesoscale processes such as blocking of an upper-level RTF ambient flow or acceleration by a midlevel mesolow.

Thus, examination of the large-scale flow should help reveal why an RTF current occurs in the southern segment of the squall line but not in its northern part. Figure 15 shows that the squall line is actually embedded in large-scale flows with a pronounced cyclonic circulation associated with the midlevel baroclinic trough and an anticyclonic circulation ahead (also see Fig. 3). It is apparent from this flow configuration that the RTF flow component depends on the location and orientation of the squall line with respect to the large-scale curved flow. In the current case, the RTF flow tends to be stronger in the southern portion of the squall system (i.e., near the base of the trough), whereas an intense FTR flow occurs in the northern segment (i.e., near the interface between the cyclonic–anticyclonic circulations). Note that because of the length scale and relative position of the squall line with respect to the large-scale cyclonic vorticity center, a midlevel “line-end” mesovortex is not generated near the northern end of the squall line, which is presumably a preferred location for the development of mesovortices, according to Zhang (1992) and Skamarock et al. (1994).

It should be mentioned that this large-scale influence on the development of the RTF flow was not discussed by Trier et al. (1991) and Lin and Johnson (1994), since their analyses domains (i.e., the PRE-STORM network) are too limited to see such a large- and mesoscale interaction. Nevertheless, Figs. 4d–f in Lin and Johnson (1994) do show the existence of intense midlevel RTF flow over a distance greater than 500 km behind the leading convective line, suggesting clearly the contribution of the ambient flow associated with the midlevel baroclinic trough to the existence of extensive trailing rear inflow. Therefore, the convectively generated meso-low or trough mechanism alone cannot explain the development of such a strong RTF flow ( $>16 \text{ m s}^{-1}$ ). This point has also been emphasized by Zhang and Gao (1989) and confirmed by recent idealized simulations of the extremely intense 10–11 June 1985 squall line, which could only produce half of the observed RTF flow intensity without large-scale support (Yang and Houze 1995; Gallus and Johnson 1995). This will be further discussed in section 6.

#### *b. The FTR ascending flows in the northern segment*

As can be seen from Figs. 12 and 13b, the low-level shallow FTR ascending flow in the northern segment of the squall system results from the overrunning of the large-scale southerly to southeasterly flow along the cold front. Furthermore, the grid-scale upward motion over the region is much weaker than that in the south (cf. Figs. 13a,b). This result appears to be mainly due to the lack of appreciable grid-scale convergence associated with a rear inflow jet, since the prefrontal environmental stability is similar to that to the south (see Figs. 6, 11, and 13). As a result, the upper-level warming and lower-level cooling, as shown for the southern segment in Fig. 10b, are weak in the northern portion, as is the convectively induced midlevel low-pressure zone (not shown). More significantly, these different circulation characteristics seem to account for the development of different weather conditions, namely, the well-organized, long-lived MCS and upper-level stratiform cloudiness in the south versus the shorter-lived MCS and the two possible layers (i.e., at middle and upper levels) of cloudiness in the northern segment. In particular, the northern precipitation appears to develop with processes different from the upper-level stratiform region that occurred in the southern squall system, although they both take place in FTR ascending flows. Specifically, the FTR transport of high- $\theta_e$  air tends to generate weak potential instability above the frontal zone (Fig. 13b), causing the development of the midlevel cloudiness. Although it is not possible to verify this phenomenon owing to the limited resolution of observations, it has been noticed in other midlatitude frontal precipitation cases (e.g., Herzegh and Hobbs 1981; Parsons and Hobbs 1983). The presence of two cloud layers suggests that the precipitation in the midlevel

clouds may involve “seeding” from above by ice particles (Cunningham 1951; Herzegh and Hobbs 1981).

#### *c. Discussion*

The above results clearly show that the large-scale circulations can play an important role in determining the squall’s internal (meso- $\beta$ -scale) structures at different portions of the system, especially in the formation of low- to midlevel RTF and FTR flows. For a similar reason, the extent of upper-level FTR outflows may depend on the orientation of a squall line with respect to the direction and intensity of larger-scale flow aloft. The current finding of the large-scale control is significant, since previous studies have shown the important roles of elevated rear inflow jets and FTR ascending flow in determining the development and distribution of precipitation and surface phenomena within a squall system (see Zhang and Gao 1989; Weisman 1992; Gallus and Johnson 1995). Specifically, the presence of an elevated and descending rear inflow jet has been shown to help increase mesoscale convergence or vertical motion, which frequently leads to the concentration of cyclonic vorticity (associated with midlevel mesolows) through tilting of horizontal vorticity and vortex stretching (Smull and Houze 1985, 1987; Zhang 1992) and to the development of surface wake lows and “gust” winds (Johnson and Hamilton 1988; Rutledge et al. 1988; Zhang et al. 1989). The midlevel mesovortex (or meso-low) will clearly in turn reinforce the RTF flow to the south (see Zhang 1992). On the other hand, the FTR ascending flow is often correlated with the formation of trailing stratiform precipitation (Houze et al. 1989; Zhang and Gao 1989; Biggstaff and Houze 1991a; Braun and Houze 1994). Therefore, if high-resolution NWP models could predict reasonably well the location of squall lines with respect to tropospheric large-scale or short-wave disturbances, a significant improvement in quantitative precipitation forecasts (QPFs) and severe weather warnings may be achieved.

In fact, a literature survey of observational studies reveals that an intense rear inflow jet occurs frequently in squall lines with favorable larger-scale circulations. For example, rear inflow jets have been observed near the base of deep mid- to upper-level troughs (e.g., Ogura and Liou 1980; Chang et al. 1981; Kessinger et al. 1987) and midlevel short-wave troughs (e.g., Leary and Rappaport 1987; Johnson and Hamilton 1988), in easterly wave troughs (e.g., Zipser 1969; Houze 1977), and in regions of midlevel westerly flow (e.g., Fankhauser et al. 1992). After all, midlatitude squall lines tend to develop in association with moderate to intense baroclinic disturbances, as distinguished from other types of MCSs (Maddox 1980b) and airmass storms. Evidently, the large-scale RTF (FTR) descending (ascending) flow can also exert important influences on the meso- $\gamma$ -scale structures and evolution of deep convection. It is unclear, however, to what extent the convective-scale cir-

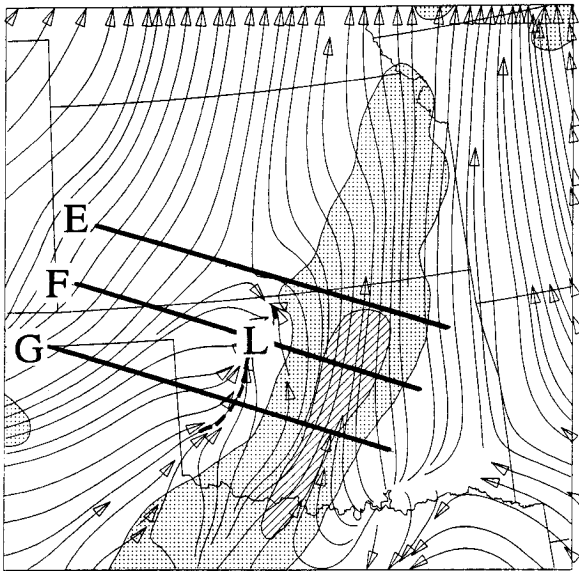


FIG. 16. Horizontal map of 500-hPa system-relative streamlines from 18-h integration (27/06–18). Letter “L” shows the position of the mesolow. Shadings show the parameterized rainfall rates with contours of 1 and 5 mm h<sup>-1</sup>.

culations could be modified by such preexisting larger-scale (RTF–FTR) flows, since most of the previous cloud modeling studies only assumed near-vanishing system-relative flows overlying a sheared boundary layer (e.g., Thorpe et al. 1982; Rotunno et al. 1988; Lafore and Moncrieff 1989). Obviously, to provide a complete understanding of the multiscale interactive processes in the current case, one has to run a numerical model with a grid size that is small enough to resolve individual convective cells but with a domain that is sufficiently large to include the midlevel traveling short-wave trough.

**6. Along-line variability due to mesoscale circulation**

As previously shown, there are two scales of circulations affecting the along-line variability of the current squall system: the baroclinically driven large-scale and the convectively generated mesoscale disturbances, particularly during the mature to decaying stages (see Fig. 8). In this section we focus only on the along-line variability of the squall’s circulations due to the convectively induced midlevel mesolow and upper-level mesohigh, although the large-scale flow always exerts an important influence on the structure and evolution of the squall system.

It is evident from Fig. 16 that corresponding to the midlevel mesolow, there is an elongated zone of confluence (or convergence) between the FTR and RTF flows that is superposed on the large-scale cyclonic flow in the trailing stratiform region. Moreover, streamlines exhibit greater curvature in the vicinity of the mesolow,

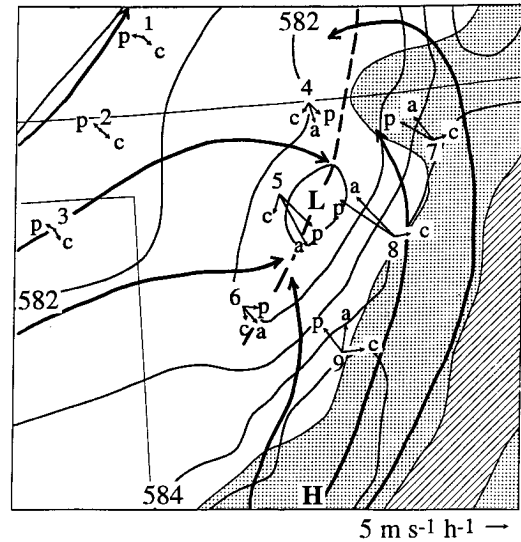


FIG. 17. As in Fig. 16 but for heights (solid, every 1 dam) superposed with system-relative streamlines (thick solid). Force balances at a few selected points are depicted, with the letters “c,” “p,” and “a” denoting the Coriolis (i.e.,  $-f\mathbf{k} \times \mathbf{v}'$ ), pressure gradient force (i.e.,  $-\nabla\phi - f\mathbf{k} \times \mathbf{c}$ ), and Lagrangian acceleration (i.e.,  $d\mathbf{v}'/dt$ ), respectively. Shadings represent the convective rainfall rates with contours of 1 and 5 mm h<sup>-1</sup>.

indicating the generation of three-dimensional meso- $\beta$ -scale structures associated with the squall convection. To help gain insight into the relationship between the mesolow and the along-line variability, horizontal momentum budgets at 500 hPa are calculated with the Lagrangian momentum equation

$$\frac{d\mathbf{v}'}{dt} = -f\mathbf{k} \times \mathbf{v}' - (\nabla\phi + f\mathbf{k} \times \mathbf{c}), \quad (1)$$

where  $\mathbf{v}'$  is the horizontal wind vector relative to the squall line,  $f$  is the Coriolis parameter,  $\mathbf{k}$  is the unit vector in the vertical direction,  $\phi$  is the geopotential height, and  $\mathbf{c}$  is the propagation vector of the squall line. Equation (1) represents a horizontal force balance among the inertial acceleration, the Coriolis force, and the pressure gradient force (PGF) in the framework relative to the squall line. Note that the term  $f\mathbf{k} \times \mathbf{c}$  has been included in the PGF calculation because of the use of the system-relative framework. Note also that the effect of numerical diffusion has been neglected in Eq. (1).

Figure 17 presents a 500-hPa map of geopotential heights and a few system-relative streamlines taken from Fig. 16 superposed with force-balance diagrams at some selected points in the vicinity of the squall system. The basic flow patterns at 500 hPa resemble those at 700 hPa (cf. Figs. 8b and 17), except that the convectively generated mesohigh becomes more evident at higher levels (see Fig. 10a). One can see that air parcels far behind the squall line (e.g., at points 1–3) are influenced little by the convectively induced pressure perturbations; they are almost in a geostrophically

balanced state with the larger-scale trough. For air parcels closer to the mesolow, however, the situation is quite different. Specifically, these parcels are forced by PGF to accelerate into the low pressure zone, while the Coriolis force tends to deflect them rightward (e.g., at points 4–9). Thus the PGF forces them to converge along the mesotrough axis, while the Coriolis force causes the parcels in the large-scale RTF southwesterly (FTR southerly) flow to be accelerated toward the south (north) of the mesolow (cf. Figs. 16 and 17). This reveals that the mesolow mechanism is indeed operative during the mature to decaying stages, as discussed by Trier et al (1991) and Lin and Johnson (1994). However, because of the presence of intense vertical motion and strong vertical shear in the vicinity of the mesolow, the midlevel mesoscale rear inflow could be viewed as part of a mesovortex circulation that results from the downward transport of the large-scale RTF momentum aloft (see Gao et al. 1990; Gallus and Johnson 1992) and the enhancement by both the tilting of horizontal vorticity and the vortex stretching (see Zhang 1992). It is important to point out that *this RTF downward momentum transport is driven by the sublimative–evaporative cooling* at the back edge of the stratiform region, which differs from the “blocking” hypothesis of Schmidt and Cotton (1990).

To further examine the along-line variability of the squall system due to the convectively generated perturbations, Fig. 18 compares the relative flow and PGF normal to the line between three different cross sections around the midlevel mesolow. Note that the depth of convectively generated disturbances is greater toward the south of the mesolow. As can be expected, most of the FTR and RTF accelerations occur in regions of large positive and negative PGF, respectively; the larger the PGF, the greater the FTR and RTF acceleration. This is particularly true for the cross section through *the center of the mesolow* (Fig. 18b). This result is consistent with the numerical momentum budget by Gao et al. (1990) and Gallus and Johnson (1992), who showed that PGF provides important contributions to the acceleration of both FTR and RTF flows. However, the RTF flow in the southern cross section is stronger than that in the middle one (cf. Figs. 18b,c), in spite of the presence of smaller PGF values in the region. As demonstrated in the force-balance diagrams in Fig. 17, this is due partly to *the deflection of the rear inflow* and partly to *the large-scale support*. On the other hand, the elevated RTF flow is weaker to the north of the midlevel mesolow (see Fig. 18a), similar to the findings of Zhang and Gao (1989).

While the mesolow (mesovortex) mechanism is operative during the mature stage, it is unclear how significant it is compared to the large-scale support. Thus, the net (i.e., direct and indirect) effect of the squall convection needs to be isolated from that associated

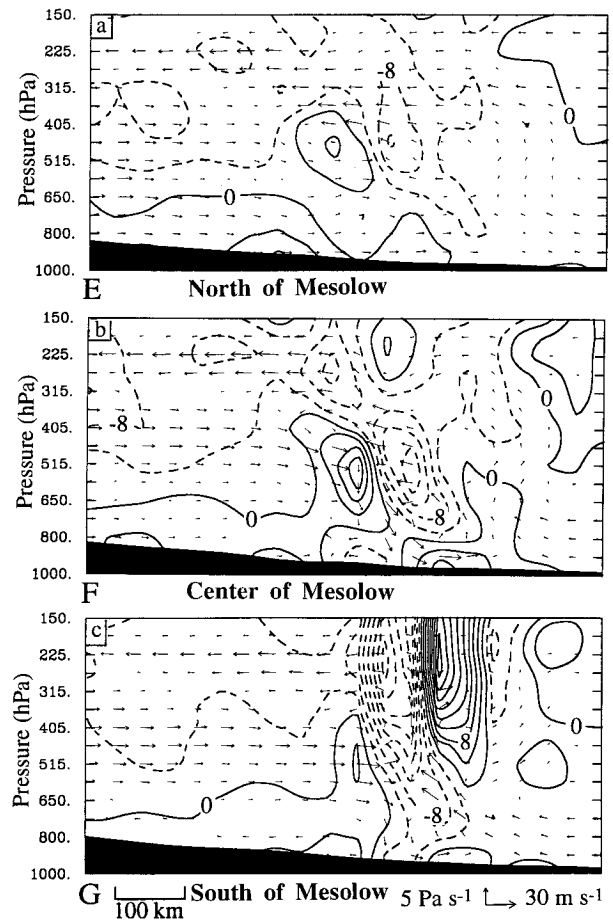


FIG. 18. As in Fig. 7 but for pressure gradient forces normal to the line (every  $4 \text{ m s}^{-1} \text{ h}^{-1}$ ) along (a) line E, (b) line F and (c) line G given in Fig. 16, which are located to the north, center, and south of the midlevel mesolow, respectively. Solid (dashed) lines are for positive (negative) values.

with the large-scale circulation by subtracting the line-normal flows in experiment DRY from those in experiment CTL. As seen in Fig. 19 the squall convection could induce, without any large-scale support, the typical two-dimensional flow structures, such as the overturning ascending flow ahead, an FTR penetrative flow into the upper-level trailing stratiform region, and an RTF flow down to the surface. However, the scale of the convectively generated RTF flow component (200 km) is much shorter than that associated with the large-scale flow (cf. Figs. 14 and 19). Moreover, the convectively generated RTF flow, on average, is about 50% to 60% of the predicted full intensity. Note, though, that part of the magnitude is caused by the phase difference of the squall lines between experiments CTL and DRY. Nevertheless, the results clearly provide further evidence on the scale interaction involved in the development of rear inflow jets as found by Zhang and Gao (1989). It is evident that both the convectively generated FTR and RTF accelerations to the south of the mesolow

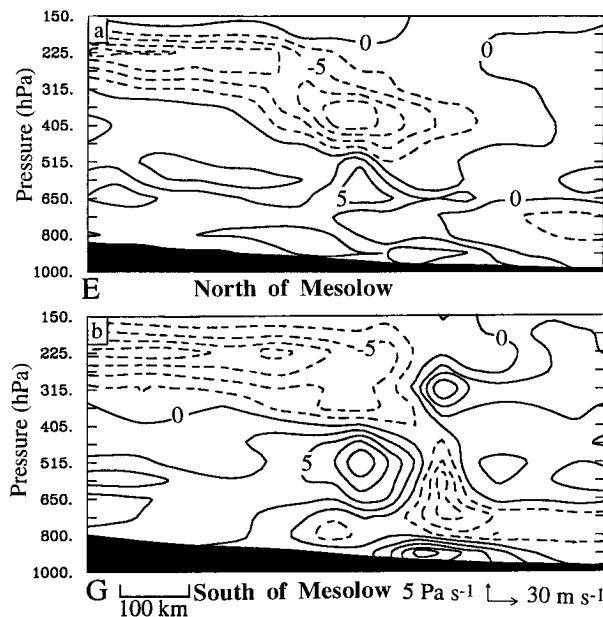


FIG. 19. Vertical cross sections of the differenced horizontal speeds (every  $2.5 \text{ m s}^{-1}$ ) normal to the line between experiments CTL and DRY that are taken from 18-h integration (27/06–18) along (a) line E and (b) line G as given in Fig. 16, which are located to the north and south of the midlevel mesolow, respectively. Solid (dashed) lines are for positive (negative) values.

are stronger than those to the north, due to the presence of more intense PGF associated with the mesohigh and mesolow. In addition, the differenced FTR flow becomes more horizontally distributed and the upper portion of the overturning flow diminishes as the cross section is shifted northward (Fig. 19a).

## 7. Summary and conclusions

In this study, an improved research version of the RFE model has been used to investigate the along-line variability of vertical circulation structures of a frontal squall line that occurred on 26–27 June 1985 during PRE-STORM. This version of the RFE model is similar to that used operationally at CMC except for the use of a high-resolution grid length and different treatments of subgrid- and grid-scale condensation. It is shown that the model reproduces reasonably well a number of basic surface features and tropospheric flow structures, as verified against available network observations. They include the initiation, propagation, and dissipation of the squall system; surface pressure perturbations and cold outflow boundaries; a midlevel mesolow and an upper-level mesohigh; an FTR ascending flow overlying an intense RTF flow; and a leading convective line followed by stratiform precipitation regions.

The across-line circulations along the northern segment of the squall line differ substantially from those along its southern segment. In particular, the classic squall-line structures that appeared in the southern seg-

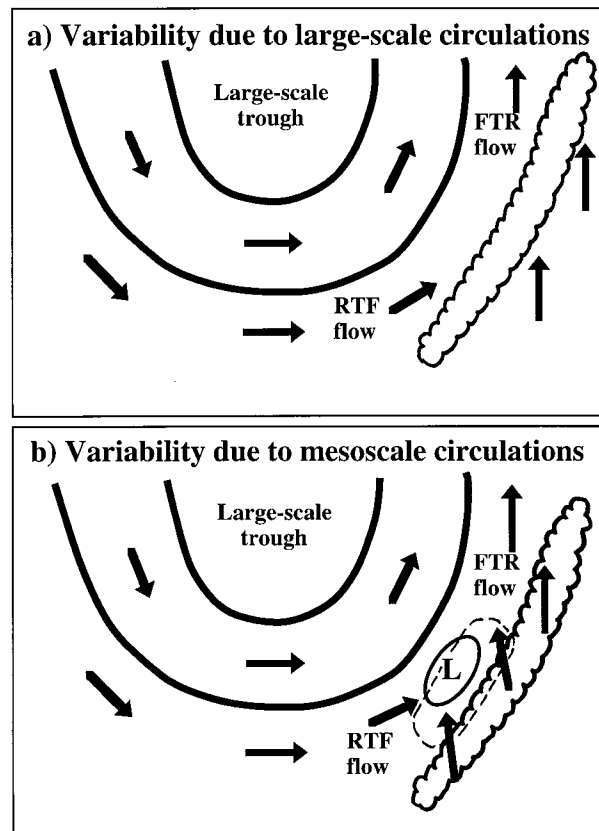


FIG. 20. Schematic representation of the influences of (a) large-scale and (b) mesoscale circulations on the internal flow structure of the squall line. The midlevel geopotential heights (thick solid) and relative flow vectors are shown. The location of the squall line (thick cloud line) and the trailing stratiform region (thin dashed) are also indicated. Letter “L” shows the position of the midlevel mesolow.

ment do not develop in the northern portion of the squall system, such as the rear inflow jet, the midlevel mesolow and surface pressure, and temperature perturbations. Instead, there are two FTR flows that are bifurcated at the leading squall front: one transports the boundary layer high- $\theta_e$  air into the upper levels and the other transports it along the frontal zone into the midtroposphere. This appears to help generate trailing cloudiness in the middle and upper parts of the troposphere.

To investigate the scale interaction involved in the development of the along-line variability, a scale separation technique is applied to the control integration and a comparison of the control run with a “dry” simulation is conducted. Both the scale analysis and the simulation comparison reveal that the along-line variability of the squall’s internal circulations results primarily from the interaction of convectively generated pressure perturbations with a midlevel baroclinic trough, as depicted in the conceptual model given in Fig. 20. This conceptual model shows that the squall’s vertical circulation structures depend on the location and orientation of the squall line with respect to the large-scale

trough and the mesoscale disturbances. Specifically, *the large-scale trough provides an extensive RTF flow component near its base* (i.e., in the southern segment) and *a favorable FTR flow component in the northern portion of the squall system* (see Fig. 20a). This large-scale contribution to the along-line variability is especially significant during the system's formative stage. In contrast, the convectively induced mesoscale disturbance tends to determine the internal circulations of the squall system in the south during the system's mature to dissipating stages (see Fig. 20b). In particular, *the midlevel mesolow (mesovortex) and upper-level mesohigh help accelerate the rear inflow jet and the divergent FTR outflow in the trailing stratiform region, respectively*. The low- to midlevel mesoscale rear inflow results from the downward transport of the larger-scale RTF momentum aloft, which is then enhanced by the mesolow or mesovortex circulation. It has been demonstrated through force-balance diagrams that the rear inflow jet tends to be more intense to the south of the mesolow (mesovortex), rather than near the center of the mesolow (mesovortex), due to the deflectional effect of the Coriolis force. This enhanced RTF flow increases the convergence and upward motion in the low to midtroposphere, thus leading to the development and organization of a more intense and longer-lived convective system in the southern segment of the squall system.

In conclusion, we may state that the vertical circulation characteristics along different parts of a midlatitude squall line are dependent on multiscale interactions, namely, from the development of deep convection to convectively generated mesoscale disturbances (e.g., mesolows and mesohighs) and large-scale circulations (e.g., baroclinic troughs and jet streams). The classic two-dimensional structures may only develop at certain, but not all, portions of squall lines. In particular, the rear inflow component, which is often correlated with organized convective development, vorticity concentration, and trailing stratiform precipitation, tends to be more intense to the south of a midlevel mesolow and near the base of a large-scale trough. In other cases, the rear inflow and upper-level FTR outflow may not develop, depending upon the distribution and orientation of squall lines with respect to their larger-scale curved flows as well as the intensity of the large-scale flows and squall convection.

Although the above conclusions are drawn from only a single squall-line study, they are more or less supported by previous studies of midlatitude squall lines. Hence, these results may have important implications for the improvement of QPFs and severe weather warnings by operational NWP models, like the one used for the current study, since some intense meso- $\beta$ -scale circulations of MCSs may be more related to meso- $\alpha$ - or larger-scale disturbances. It should be mentioned, however, that to provide an adequate understanding of the influences of the convectively generated mesolow and the larger-scale trough on the development of convective

cells along the leading line, one has to run a numerical model with a grid size that is small enough to resolve individual convective clouds but has an integration domain that is large enough to include the evolution of the midlevel baroclinic trough.

*Acknowledgments.* We are grateful to Dr. Stan Trier of the National Center for Atmospheric Research for providing Fig. 8a, and to Drs. Jocelyn Mailhot, Michel Béland, and Andrew Staniforth of Recherche en prévision numérique/Atmospheric Environment Service for their continuing interest and generous support during the course of this research. Thanks also go to Michel Valin, Bernard Bilodeau, Ning Bao, and Mario Lépine for their kindly assistance, and to Michel Riffiod of Météo-France/Centre National de Recherches Météorologiques (CNRM) for his drafting assistance. This research was funded by Environment Canada Contract KM156-0-9029, and by Natural Science and Engineering Research Council of Canada (NSERC). The first author (S. Bélair) was also supported by a graduate fellowship from NSERC.

#### REFERENCES

- Bartels, D., and R. A. Maddox, 1991: Midlevel cyclonic vortices generated by mesoscale convective systems. *Mon. Wea. Rev.*, **119**, 104–118.
- Bélair, S., D.-L. Zhang, and J. Mailhot, 1994: Numerical prediction of the 10–11 June 1985 squall line with the Canadian regional finite-element model. *Wea. Forecasting*, **9**, 157–172.
- , —, and —, 1995: Numerical prediction of an intense convective system associated with the July 1987 Montreal flood. Part I: Gravity waves and the squall line. *Atmos.–Ocean*, **33**, 447–473.
- Biggerstaff, M. I., and R. A. Houze Jr., 1991a: Kinematic and precipitation structure of the 10–11 June 1985 squall line. *Mon. Wea. Rev.*, **119**, 3034–3065.
- , and —, 1991b: Midlevel vorticity structure of the 10–11 June 1985 squall line. *Mon. Wea. Rev.*, **119**, 3066–3079.
- Brandes, E. A., 1990: Evolution and structure of the 6–7 May 1985 mesoscale convective system and associated vortex. *Mon. Wea. Rev.*, **118**, 109–127.
- Braun, S. A., and R. A. Houze Jr., 1994: The transition zone and secondary maximum of radar reflectivity behind a midlatitude squall line: Results retrieved from Doppler radar data. *J. Atmos. Sci.*, **51**, 2733–2755.
- Carbone, R. E., J. W. Conway, N. A. Crook, and M. W. Moncrieff, 1990: The generation and propagation of a nocturnal squall line. Part I: Observations and implications for mesoscale predictability. *Mon. Wea. Rev.*, **118**, 26–49.
- Chang, C. B., D. J. Perkey, and C. W. Kreitzberg, 1981: A numerical case study of the squall line of 6 May 1975. *J. Atmos. Sci.*, **38**, 1601–1615.
- Cunning, J. B., 1986: The Oklahoma–Kansas preliminary regional experiment for STORM-Central. *Bull. Amer. Meteor. Soc.*, **67**, 1478–1486.
- Cunningham, R. M., 1951: Some observations of natural precipitation processes. *Bull. Amer. Meteor. Soc.*, **32**, 334–343.
- Davis, C. A., and M. L. Weisman, 1994: Balanced dynamics of mesoscale vortices produced in simulated convective systems. *J. Atmos. Sci.*, **51**, 2005–2030.
- Dudhia, J., 1989: Numerical study of convection observed during the winter monsoon experiment using a mesoscale two-dimensional model. *J. Atmos. Sci.*, **46**, 3077–3107.
- Fankhauser, J. C., G. M. Barnes, and M. A. LeMone, 1992: Structure

- of a midlatitude squall line formed in strong unidirectional shear. *Mon. Wea. Rev.*, **120**, 237–260.
- Fritsch, J. M., and C. F. Chappell, 1980: Numerical prediction of convectively driven mesoscale pressure line. Part I: Convective parameterization. *J. Atmos. Sci.*, **37**, 1722–1733.
- , and R. A. Maddox, 1981a: Convectively driven mesoscale weather systems aloft. Part I: Observations. *J. Appl. Meteor.*, **20**, 9–19.
- , and —, 1981b: Convectively driven mesoscale weather systems aloft. Part II: Numerical simulations. *J. Appl. Meteor.*, **20**, 20–26.
- , and J. M. Brown, 1982: On the generation of convectively driven mesohighs aloft. *Mon. Wea. Rev.*, **110**, 1554–1563.
- Gallus, W. A., and R. H. Johnson, 1992: The momentum budget of an intense midlatitude squall line. *J. Atmos. Sci.*, **49**, 422–450.
- , and —, 1995: The dynamics of circulations within the trailing stratiform regions of squall lines. Part I: The 10–11 June PRE-STORM system. *J. Atmos. Sci.*, **52**, 2161–2187.
- Gao, K., D.-L. Zhang, M. W. Moncrieff, and H.-R. Cho, 1990: Mesoscale momentum budget in a midlatitude squall line: A numerical case study. *Mon. Wea. Rev.*, **118**, 1011–1028.
- Hane, C. E., C. J. Kessinger, and P. S. Ray, 1987: The Oklahoma squall line of 19 May 1977. Part II: Mechanisms for maintenance of the region of strong convection. *J. Atmos. Sci.*, **44**, 2866–2883.
- Herzogh, P. H., and P. V. Hobbs, 1981: The mesoscale and microscale structure and organization of clouds and precipitation in midlatitude cyclones. IV: Vertical air motions and microphysical structures of prefrontal surge clouds and cold frontal clouds. *J. Atmos. Sci.*, **38**, 1771–1784.
- Houze, R. A., Jr., 1977: Structure and dynamics of a tropical squall-line system. *Mon. Wea. Rev.*, **105**, 1540–1567.
- , S. A. Rutledge, M. I. Biggerstaff, and B. F. Smull, 1989: Interpretation of Doppler radar displays of midlatitude mesoscale convective lines. *Bull. Amer. Meteor. Soc.*, **70**, 608–619.
- Hsie, E.-Y., R. A. Anthes, and D. Keyser, 1984: Numerical simulation of frontogenesis in a moist atmosphere. *J. Atmos. Sci.*, **41**, 2581–2594.
- Johnson, R. H., and P. J. Hamilton, 1988: The relationship of surface pressure features to the precipitation and airflow structure of an intense midlatitude squall line. *Mon. Wea. Rev.*, **116**, 1444–1472.
- Kessinger, C. J., P. S. Ray, and C. E. Hane, 1987: The Oklahoma squall line of 19 May 1977. Part I: A multiple Doppler analysis of convective and stratiform structure. *J. Atmos. Sci.*, **44**, 2840–2864.
- Klimowski, B. A., 1994: Initiation and development of rear inflow within the 28–29 June 1989 North Dakota mesoconvective system. *Mon. Wea. Rev.*, **122**, 765–779.
- Lafore, J.-P., and M. W. Moncrieff, 1989: A numerical investigation of the organization and interaction of the convective and stratiform regions of tropical squall lines. *J. Atmos. Sci.*, **46**, 521–544.
- Leary, C. A., and E. N. Rappaport, 1987: The life cycle and internal structure of a mesoscale convective complex. *Mon. Wea. Rev.*, **115**, 1503–1527.
- Lin, X. L., and R. H. Johnson, 1994: Heat and moisture budgets and circulation characteristics of a frontal squall line. *J. Atmos. Sci.*, **51**, 1661–1681.
- Maddox, R. A., 1980a: An objective technique for separating macroscale and mesoscale features in meteorological data. *Mon. Wea. Rev.*, **108**, 1108–1121.
- , 1980b: Mesoscale convective complexes. *Bull. Amer. Meteor. Soc.*, **61**, 1374–1387.
- , D. J. Perkey, and J. M. Fritsch, 1981: Evolution of upper tropospheric features during the development of a mesoscale convective complex. *J. Atmos. Sci.*, **38**, 1664–1674.
- Moncrieff, M. W., 1981: A theory of organized steady convection and its transport properties. *Quart. J. Roy. Meteor. Soc.*, **107**, 29–50.
- Newton, C. W., and J. C. Fankhauser, 1964: On the movements of convective storms, with emphasis on size discrimination in relation to water-budget requirement. *J. Appl. Meteor.*, **3**, 651–668.
- Ogura, Y., and M.-T. Liou, 1980: The structure of a midlatitude squall line: A case study. *J. Atmos. Sci.*, **37**, 553–567.
- Orlanski, I., 1975: A rational subdivision of scales for atmospheric processes. *Bull. Amer. Meteor. Soc.*, **56**, 527–530.
- Parsons, D. B., and P. V. Hobbs, 1983: The mesoscale and microscale structure and organization of clouds and precipitation in midlatitude cyclones. IX: Some effects of orography on rainbands. *J. Atmos. Sci.*, **40**, 1930–1949.
- Rotunno, R., J. B. Klemp, and M. L. Weisman, 1988: A theory for strong, long-lived squall lines. *J. Atmos. Sci.*, **45**, 463–485.
- Rutledge, S. A., R. A. Houze Jr., M. I. Biggerstaff, and T. Matejka, 1988: The Oklahoma–Kansas mesoscale convective system of 10–11 June 1985: Precipitation structure and single-Doppler radar analysis. *Mon. Wea. Rev.*, **116**, 1409–1430.
- Schmidt, J. M., and W. R. Cotton, 1990: Interactions between upper and lower tropospheric gravity waves on squall line structure and maintenance. *J. Atmos. Sci.*, **47**, 1205–1222.
- Skamarock, W. C., M. L. Weisman, and J. B. Klemp, 1994: Three-dimensional evolution of simulated long-lived squall lines. *J. Atmos. Sci.*, **51**, 2563–2584.
- Smull, B. F., and R. A. Houze Jr., 1985: A midlatitude squall line with a trailing region of stratiform rain: Radar and satellite observations. *Mon. Wea. Rev.*, **113**, 117–133.
- , and —, 1987: Rear inflow in squall lines with trailing stratiform precipitation. *Mon. Wea. Rev.*, **115**, 2869–2889.
- Srivastava, R. C., T. J. Matejka, and T. J. Lorello, 1986: Doppler radar study of the trailing anvil region associated with a squall line. *J. Atmos. Sci.*, **43**, 356–377.
- Stirling, J., and R. M. Wakimoto, 1989: Mesoscale vortices in the stratiform region of a decaying midlatitude squall line. *Mon. Wea. Rev.*, **117**, 452–458.
- Thorpe, A. J., M. J. Miller, and M. W. Moncrieff, 1982: Two-dimensional convection in non-constant shear: A model of midlatitude squall lines. *Quart. J. Roy. Meteor. Soc.*, **108**, 739–762.
- Trier, S. B., D. B. Parsons, and J. E. H. Clark, 1991: Environment and evolution of a cold-frontal mesoscale convective system. *Mon. Wea. Rev.*, **119**, 2429–2455.
- Weisman, M. L., 1992: The role of convectively generated rear-inflow jets in the evolution of long-lived mesoconvective system. *J. Atmos. Sci.*, **49**, 1826–1847.
- , 1993: The genesis of severe, long-lived bow echoes. *J. Atmos. Sci.*, **50**, 645–670.
- Yang, M.-J., and R. A. Houze Jr., 1995: Multicell squall-line structures as a manifestation of vertically trapped gravity waves. *Mon. Wea. Rev.*, **123**, 641–661.
- Zhang, D.-L., 1989: The effect of parameterized ice microphysics on the simulation of vortex circulation with a mesoscale hydrostatic model. *Tellus*, **41A**, 132–147.
- , 1992: The formation of a cooling-induced mesovortex in the trailing stratiform region of a midlatitude squall line. *Mon. Wea. Rev.*, **120**, 2763–2785.
- , and J. M. Fritsch, 1986: Numerical simulation of the meso- $\beta$  scale structure and evolution of the 1977 Johnstown flood. Part I: Model description and verification. *J. Atmos. Sci.*, **43**, 1913–1943.
- , and —, 1988: A numerical investigation of a convectively generated, inertially stable, extratropical warm-core mesovortex over land. Part I: Structure and evolution. *Mon. Wea. Rev.*, **116**, 2660–2687.
- , and K. Gao, 1989: Numerical simulation of an intense squall line during 10–11 June 1985 PRE-STORM. Part II: Rear inflow, surface pressure perturbations and stratiform precipitation. *Mon. Wea. Rev.*, **117**, 2067–2094.
- , and H.-R. Cho, 1992: The development of negative moist potential vorticity in the stratiform region of a simulated squall line. *Mon. Wea. Rev.*, **120**, 1322–1341.
- , and —, 1995: Three-dimensional simulation of frontal rainbands and conditional symmetric instability in the Eady-wave model. *Tellus*, **47A**, 45–61.
- Zheng, Y., Q. Xu, and D. J. Stensrud, 1995: A numerical simulation of the 7 May 1985 mesoscale convective system. *Mon. Wea. Rev.*, **123**, 1781–1799.
- Zipsper, E. J., 1969: The role of organized unsaturated convective downdrafts in the structure and rapid decay of an equatorial disturbance. *J. Appl. Meteor.*, **8**, 799–814.